Environment-dependent fitness gains can be driven by horizontal gene transfer of transporter-encoding genes

David S. Milner[a,1], Victoria Attah[a], Emily Cook[a], Finlay Maguire[a,b], Fiona R. Savory[a], Mark Morrison[a], Carolin A. Müller[c], Peter G. Foster[d], Nicholas J. Talbot[a,2], Guy Leonard[a], and Thomas A. Richards[a,1]

[a]Biosciences, Living Systems Institute, University of Exeter, EX4 4QD Exeter, United Kingdom; [b]Faculty of Computer Science, Dalhousie University, Halifax, B3H 4R2 NS, Canada; [c]The Sir William Dunn School of Pathology, University of Oxford, OX1 3RE Oxford, United Kingdom; and [d]Department of Life Sciences, Natural History Museum, SW7 5BD London, United Kingdom

Edited by Nancy A. Moran, University of Texas at Austin, Austin, TX, and approved January 28, 2019 (received for review September 19, 2018)

Many microbes acquire metabolites in a "feeding" process where complex polymers are broken down in the environment to their subunits. The subsequent uptake of soluble metabolites by a cell, sometimes called osmotrophy, is facilitated by transporter proteins. As such, the diversification of osmotrophic microorganisms is closely tied to the diversification of transporter functions. Horizontal gene transfer (HGT) has been suggested to produce genetic variation that can lead to adaptation, allowing lineages to acquire traits and expand niche ranges. Transporter genes often encode single-gene phenotypes and tend to have low protein–protein interaction complexity and, as such, are potential candidates for HGT. Here we test the idea that HGT has underpinned the expansion of metabolic potential and substrate utilization via transfer of transporter-encoding genes. Using phylogenomics, we identify seven cases of transporter-gene HGT between fungal phyla, and investigate compatibility, localization, function, and fitness consequences when these genes are expressed in *Saccharomyces cerevisiae*. Using this approach, we demonstrate that the transporters identified can alter how fungi utilize a range of metabolites, including peptides, polyols, and sugars. We then show, for one model gene, that transporter gene acquisition by HGT can significantly alter the fitness landscape of *S. cerevisiae*. We therefore provide evidence that transporter HGT occurs between fungi, alters how fungi can acquire metabolites, and can drive gain in fitness. We propose a "transporter-gene acquisition ratchet," where transporter repertoires are continually augmented by duplication, HGT, and differential loss, collectively acting to overwrite, fine-tune, and diversify the complement of transporters present in a genome.

lateral gene transfer | protein connectivity | osmotrophy | gene ratchet | fungi

Horizontal, or lateral, gene transfer (HGT) is the movement of genetic material between reproductively isolated genomes, and operates in contrast to vertical inheritance, where genes are passed from parent to progeny. HGT events are common in prokaryotes (1, 2) and, although less common, it is becoming apparent that HGT events into eukaryotes are a significant factor (3) and contribute toward the evolution of eukaryotic microbes, including oomycetes (4–8) and fungi (9–12). Previous work has demonstrated that HGT events in eukaryotes produce genetic variation that can lead to adaptation, allowing lineages to utilize alternative nutrients, colonize new environments, and expand niche ranges (3, 10, 13–15). Furthermore, experimental characterization of the functions of horizontally acquired gene products (12, 16–24) has reinforced the hypothesis that HGT can drive adaptive potential in eukaryotes.

Transporter genes are potential candidates for acquisition by HGT as they constitute single-gene phenotypes (i.e., a single gene that encodes an entire functional trait), with the proteins they encode tending to have low protein–protein interaction complexity (12, 25). Consistent with this hypothesis, previous work has demonstrated that phenotypes can be acquired by single-gene HGTs (e.g., refs. 23, 26, and 27), and that HGTs tend to encode proteins that have a low number of protein–protein interactions (28–30). Furthermore, membrane transporter HGT events in eukaryotes have been described previously (5, 19, 31, 32), although relatively little work has been conducted to investigate the functional impact of HGT of transporter genes across fungal phyla and the subsequent consequences of gene acquisition on the fitness of recipient lineages. This analysis would, in turn, allow the examination of how differing environmental conditions can dictate whether HGT-acquired genes are maintained by selection within lineages, informing our understanding of pan-genome evolution in eukaryotic microbes, such as fungi.

Fungi are obligate osmotrophs and often perform a range of lysotrophic functions (33), feeding by secreting extracellular enzymes into the environment, degrading complex molecules, and importing the resulting nutrients into the cell (25). Transporter proteins are central to this process, allowing the uptake of simple monomers following extracellular enzymatic degradation. As such, the gain (e.g., by HGT or duplication) and loss of transporter proteins in fungi is hypothesized to be a key evolutionary process in driving niche range and influencing social interactions (25). We therefore sought to identify transporter gene HGT events in fungi, and examine the types of functional constraints such HGTs must overcome to become fixed within a recipient lineage. Here, we have identified seven instances of transporter gene HGT between fungal phyla, characterized the function of each using phenotype microarrays or genetic complementation,

Significance

Horizontal gene transfer (HGT) is the transfer of genetic information between genomes by a route other than from parent to offspring. Of particular interest here are the transfers of transporter-encoding genes, which can allow an organism to utilize a new metabolite, often via the acquisition of a single foreign gene. Here we have identified a range of HGT events of transporter-encoding genes, characterized the substrate preferences for each HGT encoded protein, and demonstrated that the gain of one of these HGTs can provide yeast with a distinct competitive advantage in a given environment. This has wide implications for understanding how acquisition of single genes by HGT can drastically influence the environments fungi can colonize.

Author contributions: D.S.M., N.J.T., and T.A.R. designed research; D.S.M., V.A., E.C., M.M., and T.A.R. performed research; C.A.M. contributed new reagents/analytic tools; D.S.M., V.A., E.C., F.M., F.R.S., P.G.F., G.L., and T.A.R. analyzed data; and D.S.M., N.J.T., G.L., and T.A.R. wrote the paper.

The authors declare no conflict of interest.

This article is a PNAS Direct Submission.

[1]To whom correspondence may be addressed. Email: d.milner@exeter.ac.uk or t.a.richards@exeter.ac.uk.

[2]Present address: The Sainsbury Laboratory, Norwich Research Park, NR4 7UH Norwich, United Kingdom.

This article contains supporting information online at www.pnas.org/lookup/suppl/doi:10.1073/pnas.1815994116/-/DCSupplemental.

Published online March 6, 2019.

and examined the fitness effects of one model HGT event using heterologous expression in *Saccharomyces cerevisiae*. These results show that single-gene transfer of transporter-encoding genes can drive environment-dependent fitness traits, demonstrating that gain and loss of "bolt-on-traits" can drive pan-genome evolution in fungi.

Results and Discussion

Identification of Transporter HGTs Between Ascomycetes and Basidiomycetes. Using phylogenomic approaches we sought to identify transporter proteins for which phylogenetic analysis identifies a tree topology consistent with recent HGT between the ascomycetes and basidiomycetes. To identify candidate HGTs, we generated a phylogeny for every protein annotated as a transporter in the *S. cerevisiae* S288c genome (34) using an automated pipeline (35). Putative HGT phylogenies were identified as tree topologies that demonstrated genes from a closely related group, the recipient, branching within a clade of distantly related taxa, the donor group (36). Amino acid sequence alignments of candidate HGTs were then subject to additional taxon sampling checks, alignment editing and site masking, maximum-likelihood phylogenetic reconstruction, and Bayes factor alternative topology tests. We chose to focus on identifying HGTs between ascomycete and basidiomycete taxa because genome sampling for these sister groups is relatively dense and they constitute established clades (37). This process identified seven protein sequence phylogenies where the tree topology is consistent with an Ascomycota–Basidiomycota HGT. Advanced genome sampling also allowed us to contrast gene synteny relationships across taxa and investigate whether candidate HGT genes are adjacent to genes of vertical ancestry, ruling out genome project contamination as an alternative explanation for the identified phylogenetic relationship in all seven cases (Dataset S1). In three cases, genome sampling of recently released data allowed for further phylogenetic analysis as additional putative recipient taxa were identified (Dataset S2). In total, five of the transfers (HGT-1, -2, -3, -4, and -7) identified were detected in two or more recipient genomes (Datasets S1 and S2), demonstrating independent sampling points of the HGT gene and providing further support that these phylogenetic relationships were not the product of genome project contamination. This additional sampling identified two further ascomycete–basidiomycete HGTs in the wider HGT-3 and HGT-6 transporter gene families (Dataset S2).

The seven HGTs identified were classified into a range of different transporter protein domain superfamilies, including: Sugar_tr, sugar transporters (Pfam00083: HGT-1 and HGT-4); LysP amino acid permeases (COG0833: HGT-2 and HGT-5); PTR2, oligopeptide transporter (Pfam00854: HGT-3); MFS, major facilitator superfamily (pfam07690 HGT-6); and OPT, oligopeptide transporter (Pfam03169: HGT-7). The phylogenies identified one basidiomycete-to-ascomycete HGT (HGT-5) and six ascomycete-to-basidiomycete HGTs (see Table 1 and Fig. 1 for summary, and Datasets S1 and S2 for phylogenetic data).

Investigation of Transporter HGT Integration Within a Model Cell Network. We propose that fixation of a transporter gene acquired by HGT must overcome three functional hurdles. First, the protein must not be toxic or incompatible with the recipient genetic background or cellular environment (i.e., the protein interaction network within the host cell). Second, the HGT-encoded protein must occupy the correct subcellular location to allow function and, finally, the transferred gene must confer a compatible function upon which selection can act, that is either neutral or beneficial to host fitness. Using *S. cerevisiae* as an expression chassis, we therefore investigated these functional constraints. First, we assessed growth of *S. cerevisiae* strains, each expressing an HGT transporter gene under the control of a constitutive GPD (TDH3) promoter and with a C-terminal His-tag (*SI Appendix*, Fig. S1). For two strains, HGT-2 and HGT-5, we were unable to detect protein expression by Western blot (*SI Appendix*, Fig. S2), putatively demonstrating that expression of the two transporters is detrimental to *S. cerevisiae* under this transcriptional load. This was consistent with poor growth rate (r) of the two strains (Fig. 2*J* and *SI Appendix*, Fig. S1), both of which had an r median value of <55% of the wild-type *S. cerevisiae* strain, containing only the empty p426-GPD vector. One reason for such poor growth may be the unregulated uptake of toxic levels of substrate into the cell. The uptake of large quantities of single amino acids, for example, has been shown to be toxic to *S. cerevisiae* (38). Both HGT-2 and HGT-5 show homology to LysP amino acid permeases (Table 1), suggesting that altered amino acid uptake may be the cause of poor growth rate when expressed in *S. cerevisiae*, and demonstrating that transferred transporters can be incompatible with foreign cellular environments, and thus represent a potential barrier to transporter HGT in certain environment, genetic, and cellular contexts.

Previous work has shown that functional HGTs tend to encode proteins exhibiting a low number of protein–protein interactions (28–30). Furthermore, transporter proteins show similar levels of protein–protein interaction complexity to previously identified bacterially derived HGTs present on the *S. cerevisiae* genome (Fig. 2 *A* and *B*) (25). Indeed, both transporter proteins and the bacterial HGT-acquired proteins show significantly lower connectivity than the remainder of the *S. cerevisiae* proteome (t test; both $P < 0.001$; normality tested using a Kolmogorov–Smirnov test) (Fig. 2*B*). To examine the projected protein–protein interaction complexity of each HGT transporter within the *S. cerevisiae* proteome, we used protein–protein interaction data (39) [based on BioGRID analysis (40)] to identify the number of interactions for each native *S. cerevisiae* transporter protein that shows shared amino acid sequence identity (>20%) (Fig. 2 *C*–*I*) to the HGT transporters. These data demonstrated that HGT-2 and HGT-5 putative LysP-encoding proteins, which are the proteins where retardation of growth is at the highest level and where production of the transporter cannot be confirmed via Western blot analysis, also have the highest number of projected protein–protein interactions within the yeast interactome (Fig. 2 *D*, *G*, and *J* and *SI Appendix*, Fig. S2). It is currently not possible to identify a significant correlation between toxicity (i.e., retardation of growth) and interaction complexity given the current sample size (Fig. 2*K*), but we suggest both factors are likely to be important in determining compatibility of transporters once transferred into a foreign cellular environment. The remaining five heterologously expressed transporters share comparatively reduced projected protein–protein interaction complexity (Fig. 2 *C*, *E*, *F*, and *H*–*J*). This pattern is consistent with the concept that HGTs are functionally viable when the protein–protein interaction complexity of the HGT protein in the recipient cell is low (28, 29).

Of the five transporter proteins for which we observed protein expression, HGT-1, -3, -4, and -6 were tagged with C-terminal superfolder GFP (sfGFP), and HGT-7 with N-terminal enhanced GFP (EGFP), to assess protein localization in *S. cerevisiae*. HGT-7 was tagged at the N terminus because PSORTII[47] analysis identified a putative C-terminal PTS1/SKL motif. HGT-1, -3, -4, and -6 showed a majority localization to the cell surface plasma membrane (Fig. 3*A*). The *Ustilago maydis* HGT-7 transporter showed limited plasma membrane localization and punctate internal cellular localization. N-terminal EGFP intracellular localization of HGT-7 was then assessed by colocalization with RFP-tagged endomembrane proteins in a library of *S. cerevisiae* strains (41). We observed evidence of colocalization with Sec13, suggesting a heterologous endoplasmic reticulum and Golgi vesicular interface localization for HGT-7 (Fig. 3*B*). This may be due to incomplete trafficking as a result of the addition of the EGFP tag, or some unknown characteristic of the *U. maydis*-derived gene product, yet the *S. cerevisiae* OPT2, which shares 25% amino acid identity with HGT-7, has previously been shown to interact with vesicles that cycle between the late Golgi and the plasma membrane (42), consistent with a heterologous vesicular function of HGT-7. These data demonstrate in vivo that localization of the four plasma-membrane proteins, and possibly the vesicular protein, is consistent with their predicted function as transporters. This provides support

Table 1. Details of transporter HGT events identified and characterized using *S. cerevisiae* heterologous expression

HGT	Accession no.	Recipient	Conserved domain	*S. cerevisiae* strain	OmniLog	Complementation	Strain source	Substrates identified
HGT-1 (*SI Appendix*, Fig. S3)	EJD44146	*Auricularia subglabra* (Basidiomycota)	pfam00083 Sugar_tr (sugar transporter)	BY4742 Δ*stl1*	X	✓	Euroscarf collection	Glycerol
HGT-1 (*SI Appendix*, Fig. S8)				EBY.VW4000	X	✓	(61)	Does not transport glucose
HGT-2	EJD38419	*Auricularia subglabra* (Exidia) (Basidiomycota)	COG0833 LysP (amino acid permease)	—	—	—	—	No expression detected
HGT-3 (Dataset S3)	XP_007862603	*Gloeophyllum trabeum* (*Heliocybe*) (Basidiomycota)	pfam00854 POT (proton-dependent oligopeptide family)	BY4742	✓	—	Euroscarf collection	L-glutamine; R-A; R-D; R-Q; R-I; R-L; R-M; R-F; R-V; I-G; I-M; L-A; L-R; L-I; L-M; L-S; M-Q; F-S; T-R; T-L; W-R; Y-A; Y-Q; V-N dipeptides (OmniLog)
HGT-3 (*SI Appendix*, Fig. S4)				BY4742 Δ*ptr2*	✓	✓	Euroscarf collection	H-L and L-A dipeptides (spot assays)
HGT-3 (*SI Appendix*, Fig. S5)								A-R; R-A; R-D; R-Q; R-L; R-S; G-R; L-A; L-R; L-M; L-S; M-R; M-Q; M-L; M-M; W-R; W-S; Y-Q; V-N dipeptides (OmniLog)
HGT-4 (Fig. 3 *C* and *D*)	XP_007868407	*Gloeophyllum trabeum* (*Heliocybe*) (Basidiomycota)	pfam00083 Sugar_tr [Sugar (and other) transporter]	EBY.VW4000	✓	✓	(61)	Mannose, glucose, galactose, xylose.
HGT-4 (Fig. 3*E*)				BY4742 Δ*suc2*	—	✓	Euroscarf collection	Does not transport sucrose
HGT-5	ODQ72208	*Lipomyces starkeyi* (Ascomycota)	COG0833 LysP (amino acid permease)	—	—	—	—	No expression detected
HGT-6 (Dataset S3)	XP_008042479	*Trametes versicolor* (Basidiomycota)	pfam07690 MFS_1 (major facilitator superfamily)	BY4742	✓	X	Euroscarf collection	L-glutamine; A-R; R-A; R-D; R-I; R-L; R-M; R-F; R-S; R-Y; R-V; I-R; L-A; L-R; L-D; L-E; L-G; L-M; L-S; M-Q; F-S; W-R; Y-Q; V-N; G-N; I-N; L-N; F-D; F-E; F-V; P-N; S-N; V-S dipeptides (OmniLog)
HGT-7 (Dataset S3)	XP_011390539	*Ustilago maydis* (*Sporisorium*; *Pseudozyma*; *Melanopsichium*; *Kalmanozyma*; *Moesziomyces*) (Basidiomycota)	pfam03169OPT (oligopeptide transporter protein)	BY4742	✓	X	Euroscarf collection	R-D; R-M; L-A; F-S; T-L; Y-A; V-N; G-N; I-N; F-D; F-E dipeptides (OmniLog)

First and second columns, HGT events of transporter-encoding genes and their respective GenBank accession numbers; third column, their recipient genomes and other recipient genomes in which these HGT events were identified (indicated in parenthesis); fourth column, conserved domain predictions; fifth column, *S. cerevisiae* strains used for characterization and the transporter substrates identified using each method; sixth and seventh columns, "X" = no, "✓" = yes,"—" = not applicable; eighth column, source of strains; ninth column, transporter substrates identified.

for the hypothesis that these proteins maintain a useful cellular address when moved into heterologous systems: that is, in a scenario analogous to that produced by HGT.

Functional Characterization of Transporter HGTs. To identify possible substrates for each HGT transporter, we used the OmniLog phenotype microarray (PM) system to compare growth and respiration of yeast strains expressing the transporter proteins across a range of different culture conditions. The OmniLog data demonstrate that HGT-3, -6, and -7 transport various dipeptides and HGT-4 transports hexose sugars (Dataset S3; all substrates detailed in Table 1). To test functional predictions based on homology searches, to validate the OmniLog data for HGT-3 and -4, and to investigate the possible substrate for HGT-1, a range of *S. cerevisiae* deletion mutants were then used for complementation assays (Table 1). We could not identify a putative compatible mutant for HGT-6 (a putative sugar phosphate transporter domain-containing protein) (Table 1) and, due to the internal membrane localization of HGT-7, we did not carry this transporter forward for complementation analysis. Briefly, these experiments identified that: (*i*) HGT-1 is a glycerol transporter, a poor primary carbon source for growth in yeast; (*ii*) HGT-3

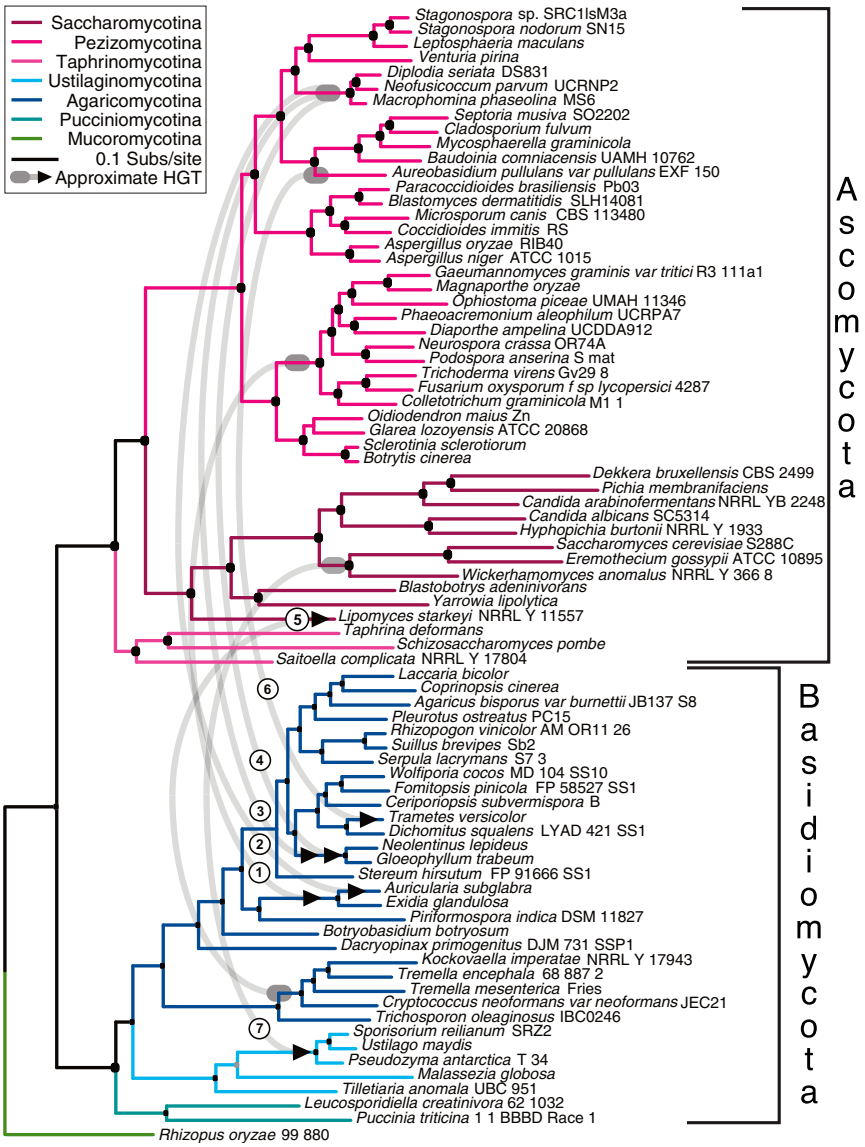

Fig. 1. Phylogeny illustrating seven transfers of predicted transporter-encoding genes. Phylogeny of published genomes showing proximate points of HGT origin and acquisition for the seven primary HGTs identified (Dataset S1). For two additional HGTs identified with increased genome sampling within HGT-3 and -6 wider gene families, see Dataset S2. The species phylogeny was calculated from an alignment of 79 taxa (Dataset S5) and 134,948 characters based on the JGI-1086 hidden Markov models (37) (https://github.com/1KFG/Phylogenomics_HMMs), using a maximum-likelihood approach in IQ-Tree v1.5.4 with LG model and 1,000 ultrafast bootstraps.

mediates uptake of 19 dipeptide substrates when expressed in the *ptr2* deletion strain (*PTR2* encodes a transporter known to facilitate dipeptide uptake) (43), of which 12 substrates were also identified in the OmniLog PM screen of strain BY4742 (Dataset S3); and (*iii*) HGT-4 uptakes the hexoses mannose, glucose, galactose, and the pentose xylose (Fig. 3 *C* and *D*), with the latter a poor primary carbon source for growth of many *S. cerevisiae* strains (44).

The hexose/pentose transporter HGT-4 exhibits key differences in amino acid sequence from *S. cerevisiae* Gal2 [the top HGT-4 BLASTP hit in *S. cerevisiae* (42% amino acid identity)] (Fig. 3*F*). A similar pattern of amino acid substitutions, primarily in the loop between transmembrane (TM) domains 6 and 7, were also identified as important for defining substrate range in directed evolution experiments, where mutagenesis of Gal2 identified sequence variants that resulted in enhanced xylose uptake (45). The relatively poor level of galactose uptake facilitated by HGT-4 (Fig. 3 *C* and *D*) is also in agreement with Kasahara et al. (46), who demonstrated that Tyr446, located within TM10 of the Gal2 protein, is essential for galactose recognition and that substitution of this residue with Phe (as observed in the same region of HGT-4) (Fig. 3*F*) results in glucose uptake. Consistent with these amino acid characteristics, HGT-4 increases *S. cerevisiae* growth rate/respiration with xylose as the sole carbon source (Fig. 3 *C* and *D*), demonstrating a dramatic phenotype difference and alteration in nutrient/environment growth dynamic with a single-gene acquisition. Interestingly, the recipients of HGT-4 are Gloeophyllaceae, brown rot fungi (Fig. 1 and Dataset S1), which play a dominant role in communities that function to decompose wood, an environment rich in xylose (47). Collectively the OmniLog and complementation data identify substrates of five heterologously expressed HGT transporter proteins (Table 1), confirming that the putative transporters function to obtain metabolites that are compatible with many fungal cellular metabolic functions (15, 48). However, both approaches are likely to underestimate the full substrate range of these transporter proteins.

Testing Environmental/Metabolic Fitness Parameters for a Model HGT. Both HGT-1 and HGT-4 significantly improve how yeast can grow on "nonfavored" carbon sources, glycerol and xylose, respectively (45, 49). This demonstrates that single HGT acquisitions when "recapitulated" in yeast can alter growth, a proxy for fitness, across nonstandard yeast culture conditions, a proxy for altered niche space. To explore this possibility, we selected the HGT-1 transporter as a model HGT acquisition to investigate environment-specific gain-of-fitness outcomes. We performed competitive fitness assays by culturing a GFP-labeled *S. cerevisiae* strain expressing HGT-1 with a BFP-labeled strain containing an

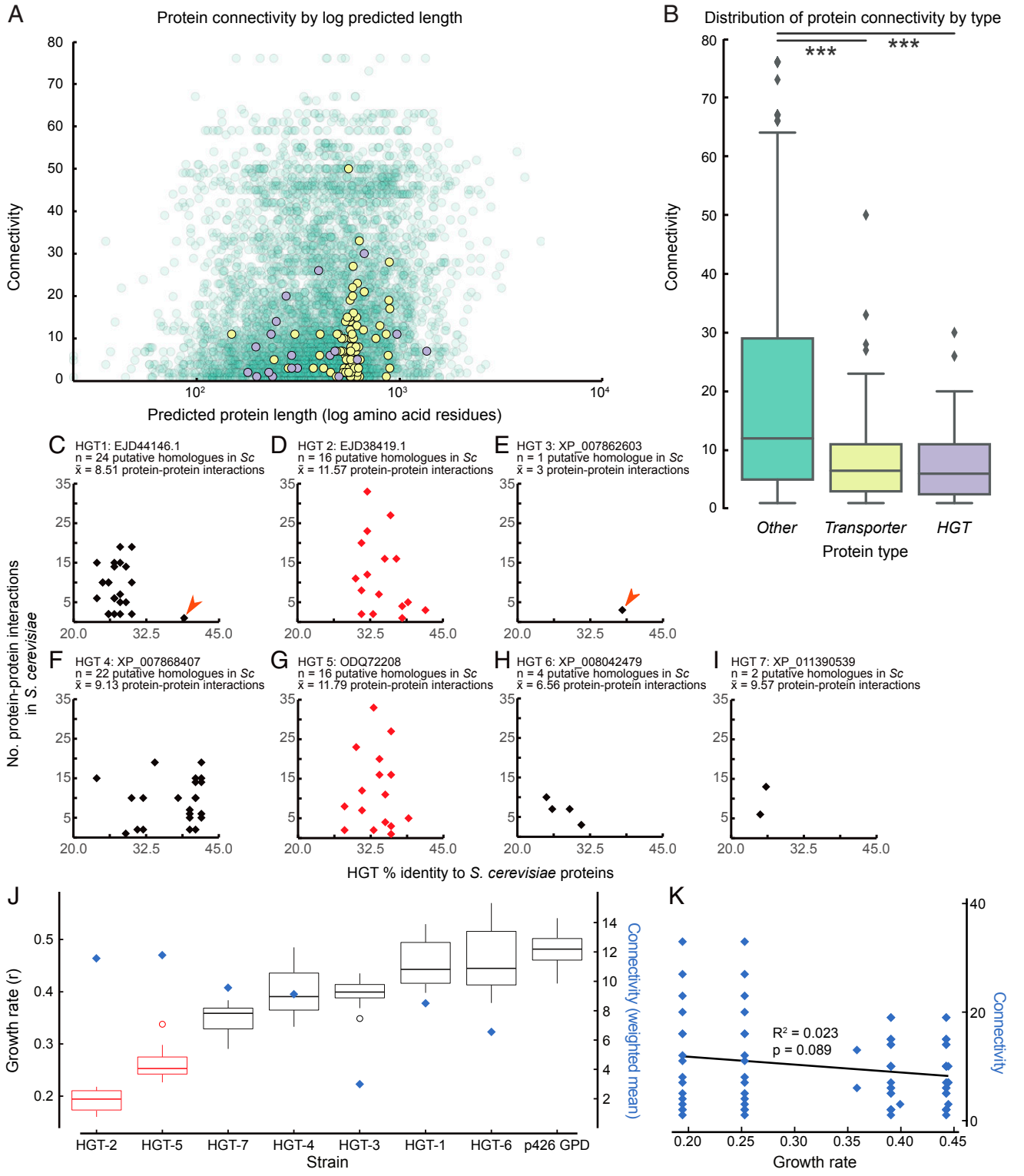

Fig. 2. *S. cerevisiae* predicted protein connectivity distribution and investigation of projected protein–protein connectivity of HGT transporters when expressed in *S. cerevisiae*. (*A*) Protein connectivity by log-predicted length for *S. cerevisiae* proteome [source data collated by Cotton and McInerney (39)]; yellow: transporter proteins; mauve: proteins acquired by HGT; green: all other *S. cerevisiae* proteins for which protein connectivity data are available. (*B*) Distribution of protein connectivity by type, showing that transporter proteins, and proteins acquired by HGT, typically show low connectivity (***$P < 0.001$). (*C–I*) Projected protein–protein interactions for the *S. cerevisiae* homologs (>20% amino acid identity) of each HGT transporter gene identified here. HGT-acquired genes that were shown to be expressed are indicated in black, while those where expression was not detected are indicated in red. Orange arrowheads indicate *S. cerevisiae* homologs validated by complementation (*C*: Stl1; *E*: Ptr2). (*J*) Box plot showing growth rates for each *S. cerevisiae* strain expressing an HGT-acquired gene, plotted against weighted mean connectivity for each group of *S. cerevisiae* homologs (blue diamonds). Circles represent outliers. (*K*) Weighted linear regression of projected protein–protein interactions for the *S. cerevisiae* homologs (>20% amino acid identity) of each HGT transporter gene vs. mean growth rate of each *S. cerevisiae* strain expressing each HGT. The regression was weighted by the squared proportional identity. Data (from ref. 39) used to generate *A* and *B* are available at doi: 10.6084/m9.figshare.6834770.

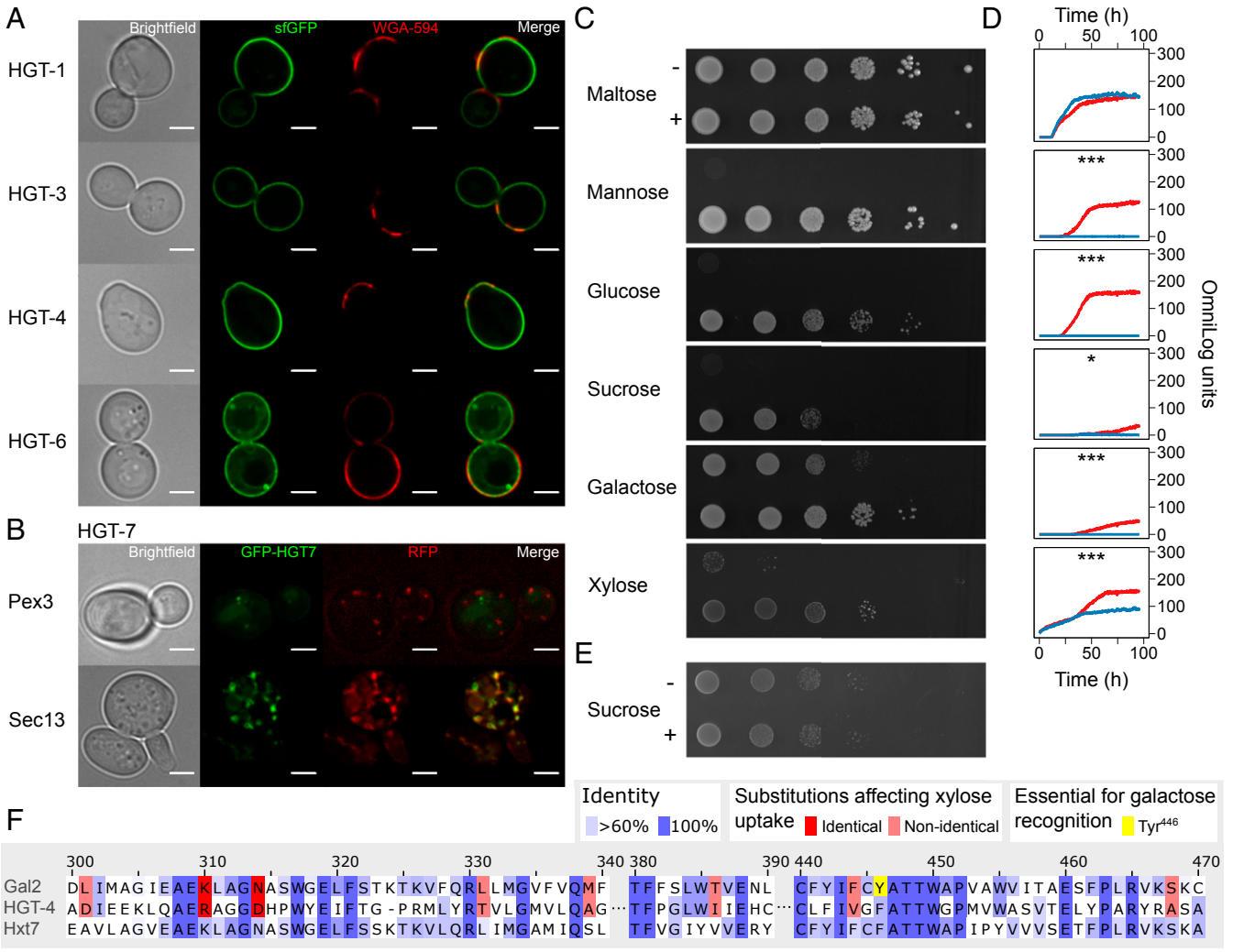

Fig. 3. Localization of HGT-acquired transporter proteins; HGT-4 complementation assays and protein sequence substitution analysis. (*A*) Localization of HGT-1, -3, -4, and -6 when labeled with sfGFP. Colocalization with the cell periphery as indicated by costaining with WGA Alexa Fluor 594 conjugate, a lectin that preferentially binds to chitin. (Scale bars, 3 μm.) (*B*) Localization of EGFP-labeled HGT-7; colocalization was observed between EGFP-HGT-7, and Sec13 (endoplasmic reticulum-to-Golgi vesicles). (Scale bars, 3 μm.) (*C*) Complementation of EBY.VW4000 hexose transporter null mutant with HGT-4 (+) or empty vector control (–) after 5-d growth (or 8 d for xylose) on different sugar sources. Dilution series from 10^0 to 10^{-5} (left to right) (*D*) OmniLog complementation of EBY.VW4000 by HGT-4, showing restoration of growth on all substrates, with maltose as a positive control: red, p423-GPD HGT-4; blue, p423-GPD empty vector (*$P < 0.05$, **$P < 0.01$, ***$P < 0.001$). (*E*) Assessing for complementation of *S. cerevisiae suc2* deletion strain with HGT-4 (+) or empty vector control (–); dilution series from 10^0 to 10^{-5} (left to right). No complementation was observed, indicating that HGT-4 does not facilitate uptake of sucrose. (*F*) Alignment of HGT-4 with Gal2 and Hxt7. Substitutions improving xylose uptake in Gal2 were identified by Reznicek et al. (45).

empty p426-GPD vector or a BFP-labeled strain expressing a native glycerol transporter, *stl1* (50) (*SI Appendix*, Fig. S6). Stl1 was selected, as this native protein sequence shared the highest level of amino acid identity with HGT-1 (39% protein identity with no other putative homologs showing similar levels of sequence identity Fig. 2*C*). The *stl1*-expressing strain was investigated to determine if any environment-specific gain-of-fitness outcomes due to HGT-1 acquisition could be achieved by comparable transcriptional rewiring and altered protein dosage of the native glycerol transporter. Quantitative Western blot analysis demonstrated that Stl1p and HGT-1 protein expression was equivalent (*SI Appendix*, Fig. S7). Strains were cocultured in media with either glycerol or glucose as the sole carbon source, or an equal mix (wt/vol) of both glycerol and glucose. For each strain, relative abundance was monitored over time using flow cytometry and a measurement at the 72-h time point was used to determine the relative population dominance as a proxy for fitness.

A significant growth advantage was observed for the strain expressing HGT-1 when incubated in 1–5% glycerol with either the empty p426-GPD or p426-GPD Stl1 strain (all $P < 0.001$, generalized linear model with binomial error distribution) (Fig. 4*A*). This demonstrates an environment-specific gain-of-fitness that is not simply the product of altered transcription of the resident glycerol transporter gene. In the presence of 0.1% glycerol, the HGT-1–expressing strain exhibited similar "fitness" to the empty p426-GPD vector strain, but was at a disadvantage when cocultured with the p426-GPD Stl1 strain (all $P < 0.001$) (Fig. 4*A*). When cells were grown in glucose or in a glycerol/glucose mix, or when the carbon source was switched every 12 h, there was a significant disadvantage for those expressing HGT-1 relative to those containing only the empty p426-GPD vector ($P < 0.001$ at all substrate concentrations tested) (Fig. 4 *B*–*D*). This is likely to be a consequence of the cost of expressing the HGT-1 protein (Fig. 2*J*) and points toward a requirement for environmental-specific selection for fixation of the HGT transporter under a given promoter and, therefore, specific transcriptional load. It could also, however, be the result of differences in transcription because the constitutive GPD promoter may behave

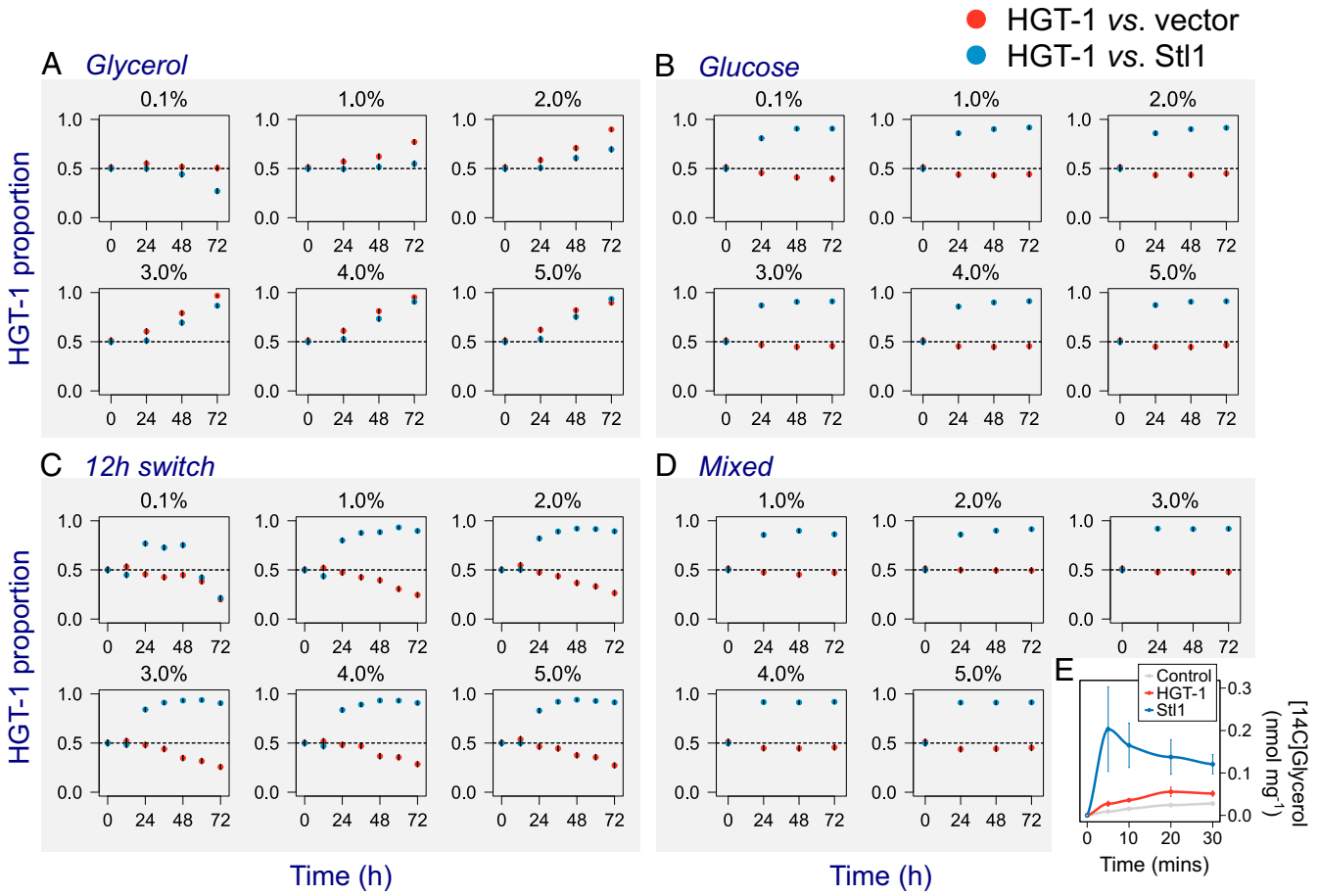

Fig. 4. HGT-1 competitive fitness assays and glycerol uptake kinetics. (*A–D*) Proportion of *S. cerevisiae* cells expressing HGT-1 when competed against a p426-GPD vector-only control (red) or against a *S. cerevisiae* strain expressing the native transporter, Stl1 (blue). Experiments were performed over a 72-h time-period, where glycerol (*A*) or glucose (*B*) were provided as the sole carbon source, when glycerol and glucose were alternated at 12-h intervals (*C*: 12-h switch between substrates), or when a combination of glycerol and glucose (*D*: mixed) were provided as the carbon source. Points represent the mean proportions of live cells from three replicates; error bars represent SEs, obtained from a generalized linear model with binomial error distribution. Horizontal dashed lines correspond to starting proportions (0.5), when genotypes were present at equal frequencies. (*E*) ^{14}C glycerol accumulation of *S. cerevisiae* with either empty vector (p426-GPD) or HGT-1, Stl1 vectors. Greater and more rapid accumulation was observed for the strain expressing *stl1* than for *HGT-1*.

differently under each nutrient condition. Nevertheless, overexpression of HGT-1 was advantageous relative to overexpression of Stl1 (under the same promoter) when cells were grown in glucose or a glycerol/glucose mix, and when the carbon source was switched every 12 h ($P < 0.001$ at all concentrations tested) (Fig. 4 *B–D*), suggesting a greater cost of Stl1 expression in nonsubstrate and mixed substrate environments (confirmation that glucose is not a substrate of HGT-1 or Stl1 is shown in *SI Appendix*, Fig. S8). Interestingly, radiolabeled glycerol accumulation assays demonstrated a higher uptake rate of glycerol by the Stl1 transporter compared with the HGT-1 transporter (Fig. 4*E*), suggesting that the advantage of HGT-1 in 1–5% glycerol (Fig. 4*A*) is a product of the gain of a transporter with a moderate substrate uptake rate (Fig. 4*E*), compared with the resident xenologous transporter.

Conclusion: Transporter Gene Repertoires Are Subject to a Gene-Acquisition/Loss Ratchet. Collectively, these results illustrate scenarios where transporter proteins are gained, depending on a chance gene acquisition by HGT, followed by environmental selection to drive fixation of the newly acquired trait. In contrast, absence of selection can result in loss of both native transporters and HGT-acquired transporters by drift. The data presented here show that fixation of a transporter HGT is not just a property of altered substrate range, but also a consequence of acquisition of a transporter with different uptake kinetics. Collective cellular transporter function is therefore under selection for continual changes in protein function brought on by changes in the environment, including the opportunity for niche expansion and the inherent instability of environmental substrate concentrations. Consequently, selection and drift will continually drive the reconfiguration of transporter complements, causing complex patterns of phylogenetic inheritance within transporter gene families, where acquisition of transporters can continually augment or overwrite the resident transporter repertoire, essentially operating as a gene-acquisition ratchet (Fig. 5). This ratchet renders phylogenetic tree topologies of transporter gene families highly discontinuous, as is observed for many such gene families (51–53). This ratchet and the discontinuity of transporter gene family evolution has important implications for understanding how microbial pan-genomes evolve and how microbes colonize new and variant environments, including host environments where colonization is a precursor to disease.

Materials and Methods

Identification and Phylogenetic Analysis of Transporter HGTs. Using the annotated yeast proteome (39), we used BLAST2GO, TMHMM, and PFAM annotations to identify candidate transporter gene families. For each candidate transporter we used BLASTp searches (conducted using iterative gathering thresholds in a range between $1e^{-50}$ to $1e^{-10}$) of a custom-built database of 160 fungal genomes (Dataset S4) to sample a diverse collection of putative transporter protein homologs. BLASTp searches were conducted separately for each individual genome in the gene database to maximize

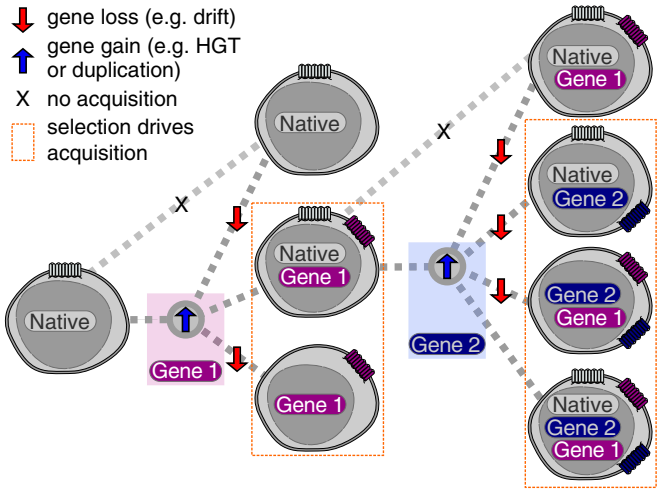

Fig. 5. Schematic figure showing alternative outcomes arising from HGT of genes encoding transporter proteins and demonstrating alternative scenarios that drive a transporter gene transfer ratchet.

recovery of candidate protein homologs from each genome. Phylogenies were generated for each set of transporter gene families using a custom-built pipeline (35); briefly, amino acids were aligned using MAFFT (54), masked using TRIMAL v1.4 (55), and a tree was generated using FastTree2 (56) using an SH-like aLRT method for assessing topology support. Trees were then manually inspected for evidence of HGT between ascomycetes and basidiomycetes. Putative HGTs were identified when closely related groups of ascomycete transporter genes and taxa (i.e., the recipient group) branched within a diverse clade of basidiomycete genes (i.e., the donor group), or vice versa. The resulting alignments were then manually edited to remove distant paralogues (determined from the phylogenetic tree) and any highly similar sequences from the same genus/groups. These sequences were then BLASTp-searched against the National Center for Biotechnology Information *nr* database and the JGI Mycocosm portal (as of May 2018) to check for missing taxon sampling (due to proteomes of taxa being released after the original analysis), the alignments were manually corrected by removing amino acid sequences with poor gene models that branched separately to the HGT donor and recipient clade, and the final alignments were masked manually to generate a refined data matrix for further phylogenetic analysis.

For the final phylogenetic analysis, we used the automatic model selection feature within IQ-Tree multicore v1.6.2 (57) to identify an appropriate substitution model using the Bayesian Information Criterion (*SI Appendix*, Table S4). This was then used to calculate a maximum-likelihood phylogeny with 200 standard bootstrap replicates (not ultrafast or fast bootstrap methods). All HGT topologies were supported with one or more nodes of ≥90%, two nodes of ≥80%, or three or more nodes of ≥50% bootstrap support for the recipient group branching within the donor group (i.e., an HGT tree-topology). Donor groups were identified based on evidence of a local ascomycete (or basidiomycete, depending on the direction of transfer) paralogue set (Datasets S1 and S2). This approach allowed us to exclude the possibility of interpreting HGTs as differentially lost ascomycete or basidiomycete paralogues. Using the same approach in IQ-Tree, we then constructed constrained phylogenies so that the tree search was prevented from searching tree topologies where the recipient group branched within the donor group (see Dataset S1 for illustration of each constrained donor group). Constraints were selected so only the donor paralogue was constrained as monophyletic. To statistically compare alternative constrained "non-HGT" topologies with unconstrained HGT topologies, we used a Bayes factor approach (58). Bayesian runs were performed for both constrained and unconstrained topology searches using P4 (59), with the sequence-substitution models shown in *SI Appendix*, Table S4. Each tree was run twice to check that the likelihood plots of the tree searches were similar, with each tree run for 400,000 generations. Convergence was assessed by examination of the likelihood plots (average marginal likelihood difference between replicate runs was 2.23, with the largest difference being 7.9). The Bayes factor B_{10} can be defined as the ratio of marginal likelihoods of alternative tree topologies (hypotheses H1 and H0), with values of $\log_e B_{10}$ interpreted as follows: 1–3 positive; 3–5 strong; >5 very strong (58). Using the approach proposed by Newton and Raftery (60) to compare marginal likelihood and identify Bayes factors for the unconstrained trees (H1) and the constrained trees (H0), we were able to demonstrate that all HGT phylogenetic relationships were robust according to established criterion for Bayes factor tests (*SI Appendix*, Fig. S9). Similar tests were applied for the phylogenies that sampled additional recently released genome data and which allowed the identification of additional putative HGT-recipients (i.e., HGT-2, -3, and -6) (Dataset S2). As part of this analysis, we used constrained vs. unconstrained tree topology analysis and Bayes factor tests to investigate whether the multiple HGT-recipient clades identified were monophyletic or paraphyletic (Dataset S2). This process identified an additional two candidate ascomycete-to-basidiomycete HGTs (HGT-3 and HGT-6).

Projecting Protein Connectivity. All *S. cerevisiae* (S288c) sequences with >20% amino acid identity according to BLASTp searches of each HGT amino acid sequence were recovered. The degree of connectivity [using BioGRID data (40), collated by Cotton and McInerney (39)] and protein identity for each BLASTp hit were then used to compute a weighted mean of the projected protein–protein connectivity for each of the HGT gene products in *S. cerevisiae*. The weighted means were calculated based on percentage protein identity of the yeast amino acid sequences with shared identity to the HGT.

Strains, Plasmids, and Culture Conditions. *S. cerevisiae* strains listed in *SI Appendix*, Table S1 were grown at 30 °C, 180 rpm. Strains were typically grown in SC medium [0.79% yeast nitrogen base without amino acids (Formedium), 700 mg L^{-1} complete supplement mix (Formedium), 2% (wt/vol) glucose, and 1.8% (wt/vol) Agar No. 2 Bacteriological (Lab M)], with dropout media used where required. Strain EBY.VW4000 (61) was grown in yeast nitrogen base without amino acids supplemented with 2% (wt/vol) maltose, 100 μg mL^{-1} leucine, 50 μg mL^{-1} tryptophan, 20 μg mL^{-1} uracil, and 20 μg mL^{-1} histidine. *S. cerevisiae* strains from the RFP-tagged library (41) were grown in the presence of G418 Sulfate (Invitrogen) at 200 μg mL^{-1}.

Cloning and Construction of Yeast Expression Plasmids. ORFs were synthesized de novo (Genewiz) and cloned into yeast expression vector p426-GPD (ATCC) with a C-terminal 6xHis tag. ORFs were also cloned into p423-GPD by digestion with SpeI and XmaI restriction enzymes (New England BioLabs) and ligation into p423-GPD (ATCC) using T4 DNA ligase (Thermo Scientific). To generate a Gateway-compatible plasmid with a C-terminal sfGFP sequence, the *attR1/ccdB/attR2* region of pAG426GPD-ccdB-EGFP was amplified using Phusion polymerase and primers attR1_BglII_F and attR2_HindIII_R (*SI Appendix*, Table S2). The resulting PCR product was digested with BglII and HindIII and cloned into the BamHI/HindIII sites of the non-Gateway p426-GPD sfGFP plasmid to generate Gateway-compatible pDM002 (pAG426 GPD *ccdB* sfGFP).

To assess localization, ORFs were amplified using primers in *SI Appendix*, Table S2 and cloned into pDONR221 using Gateway recombination (Life Technologies). The final construct was generated by mobilization into pDM002 (construction detailed above) to generate a C-terminal sfGFP construct fusion (HGT-1 to -6) or into pAG426GPD-EGFP-ccdB (62) to generate an N-terminal fusion (HGT-7). Plasmid p426-GPD *stl1* was constructed by amplification of the *stl1* gene from *S. cerevisiae* W303-1A genomic DNA using Phusion DNA polymerase and primers Stl1_SpeI_F and Stl1_XmaI_R (*SI Appendix*, Table S2). The PCR product was then digested with XmaI and SpeI and ligated into p426-GPD. For plasmid transformation, competent cells were prepared as described by Thompson et al. (63), mixed with 500-ng plasmid DNA and pulsed at 1.5 kV in an Eppendorf electroporator. Cells were suspended in YPD [20 g L^{-1} peptone bacteriological (Oxoid), 10 g L^{-1} yeast extract (Oxoid), 2% (wt/vol) glucose] and grown at 30 °C with 180 rpm shaking for 16 h before plating on the appropriate selective growth medium.

Microplate Growth Assays. *S. cerevisiae* cells (eight replicates per strain) were grown to stationary phase at 30 °C, 180 rpm, washed, and suspended in SC medium (2% glucose) lacking uracil (SC-ura) and diluted to an OD_{595} of 0.1. Cells were inoculated into a 96-well flat-bottom microplate, covered with a sterile polyester film and grown at 30 °C in a Fluostar Omega Lite microplate reader (BMG Labtech). Optical density (595 nm) was assessed at 10-min intervals, with continuous double-orbital shaking (200 rpm) between reads. Growth-curve parameters were calculated using the Growthcurver R package (64).

Western Blots. Strains were grown for 16 h at 30 °C, 180 rpm shaking and 1-mL culture was pelleted and snap-frozen in liquid nitrogen. The pellet was thawed on ice and suspended in 250-μL complete cracking buffer [480 g L^{-1} urea, 50 g L^{-1} SDS, 400 mg L^{-1} Bromophenol blue, 0.1 mM EDTA, 40 mM Tris·HCl (pH 6.8)] supplemented with 2.5 μL 2-Mercaptoethanol, 8.25 μL Pepstatin A (1 mg mL^{-1}), 0.25 μL Leupeptin (1 mg mL^{-1}), and 12.5 μL phenylmethylsulfonyl fluoride (100×). Cells were disrupted by addition of

glass beads, followed by heating at 70 °C for 10 min and homogenization in a FastPrep-24 instrument (MP Biomedicals). Cell debris was pelleted by centrifugation at 16,000 × *g* at 4 °C, the supernatant was removed, and a second extraction was performed. The supernatant was incubated at 100 °C for 2 min before protein separation on a 10% SDS/PAGE gel. Following gel electrophoresis, proteins were transferred onto a membrane in Tris-Glycine transfer buffer and the membrane was washed in TBS. The membrane was then incubated for 1 h in blocking solution (1% Alkali-soluble casein), washed twice in TBS supplemented with 0.2% Triton X-100 and 0.05% Tween-20, then once in TBS. The membrane was incubated in a 1,000-fold dilution of the His-Tag Antibody HRP-conjugate (Merck Millipore), the wash steps were repeated, and the membrane was incubated in ECL2 Western blotting substrate (Pierce) before imaging to assess the presence or absence of each His-tagged transporter protein.

Quantitative Western Blots. Quantitative Western blotting was performed based on the method of Schütz et al. (65). Briefly, strains were grown for 16 h at 30 °C, 180 rpm shaking and 4×10^7 cells (equivalent to an OD_{600} of 4) were pelleted, washed in water, and resuspended in 1 mL 2 M lithium acetate. Cells were incubated on ice for 5 min, pelleted, resuspended in 200 μL 0.4 M NaOH, and incubated on ice for an additional 5 min. Cells were then centrifuged and resuspended in 100 μL TruPAGE LDS Sample Buffer (Sigma-Aldrich) containing 50 mM DTT and incubated at room temperature for 15 min.

Proteins were separated on a TruPAGE 10% polyacrylamide gel (Sigma-Aldrich) alongside the Chameleon Duo ladder (LI-COR) and transferred onto Immobilon-FL membrane (Merck Millipore). Total protein staining was performed using REVERT Total Protein Stain (LI-COR) following the manufacturer's instructions.

The membrane was washed in PBS and blocked overnight in 0.1% Alkali-soluble Casein in 0.2× PBS. The membrane was then washed in PBS, incubated in Rabbit Anti-6X His tag antibody (ab9108; Abcam) (1:1,000) in blocking buffer +0.1% Tween20 for 1 h, washed four times in PBST, then incubated in Goat anti-Rabbit antibody conjugated to 800CW (ab216773; Abcam) (1:10,000) in blocking buffer +0.1% Tween20 for 3 h. The membrane was washed four times in PBST, then once in PBS before imaging on a LI-COR Odyssey Fc imaging system.

Phenotype Microarrays. To prepare cells for OmniLog PM plates, each yeast strain was grown on SC medium (with appropriate auxotrophic selection) at 30 °C for 48–72 h. Colonies were suspended in Yeast Nutrient Supplement (NS) solution and adjusted to an OD_{600} of 0.2. The appropriate volume of cell suspension was added to inoculating fluid specific to each PM plate type, as detailed in *SI Appendix*, Table S3. Initial PM analyses utilized yeast strain BY4742, with specific analyses using deletion strains described below. PM plates were incubated at 30 °C for 48 h or, for EBY.VW4000 strains, at 30 °C for 96 h. Each assay was performed in triplicate using three independently obtained yeast transformants.

OmniLog PM outputs were analyzed by normalizing each individual plate against well A01 (negative control) to control for any background growth as a result of the inoculation solution or metabolite carryover, then analyzed using OmniLog PM (66). Within OmniLog PM, an ANOVA model was used, with multcomp algorithms (67) within the omp_mcp function used for statistical comparisons of group means. For *S. cerevisiae* EBY.VW4000 strains, which were incubated over a longer time period, data were aggregated using the "opm-fast" method. For all other analyses, data were aggregated using the default curve parameters within the "grofit" package. For BY4742 assays, compounds where growth reached over 75 "OmniLog units" and which rescued OmniLog dye reduction to levels not significantly different to the empty vector wild-type control, were deemed to be substrates. Dipeptides containing histidine, lysine, or cysteine were excluded from these analyses, as such compounds have been shown to cause dye reduction even in the absence of growth (43).

Yeast Complementation Assays. To assess the ability of each transporter to complement yeast strains lacking specific transporter proteins, vectors were transformed into yeast strains with reported transporter gene deletions (see *SI Appendix*, Table S1 for strain information). BY4742 *ptr2Δ::KanMx* was transformed with p426-GPD or p426-GPD HGT-3. *Δptr2* transformants were grown to stationary phase in SC-ura, washed twice and suspended in water, then spotted onto SC medium (2% glucose) supplemented with complete supplement mixture lacking histidine, leucine, and uracil and 10 mM His-Leu dipeptide (Sigma Aldrich), or supplemented with complete supplement mixture lacking leucine and uracil and 1 mM Leu-Ala hydrate (Sigma Aldrich).

BY4742 *stl1Δ::KanMx* was transformed with p426-GPD, p426-GPD-HGT-1, or p426-GPD-*STL1*. BY4742 *stl1* transformants were grown to stationary phase and suspended in YPG lacking uracil [0.79% yeast nitrogen base without amino acids, 770 mg L^{-1} complete supplement mix-URA (Formedium) and 2% glycerol] at OD_{600} 0.1, and growth was observed by measuring OD_{600}.

S. cerevisiae strain EBY.VW4000 was transformed with p423-GPD or p423-GPD-HGT-4 and selected on YNB medium (yeast nitrogen base without amino acids supplemented with leucine, tryptophan, and uracil), 2% maltose. Transformants were grown in the same medium, washed once, and diluted to OD_{600} 1.0 in water, and a dilution series was spotted onto YNB medium supplemented with 2% sugar. Growth was assessed after 5-d incubation at 30 °C. Xylose plates were assessed after 8-d incubation. The same was done for *S. cerevisiae suc2* strains (a mutant that is not able to secrete invertase to catalyze breakdown of sucrose to hexose subunits), and were spotted onto YNB medium supplemented with leucine, lysine, uracil, and 2% sucrose. This was done to assess whether the HGT-transporter could transport sucrose. Each image is representative of the three biological replicates performed. *S. cerevisiae* strain EBY.VW4000 was also transformed with p426-GPD-HGT-1 and p426-GPD-*STL1* to assess growth on 2% glucose (as above). Growth was assessed after 5-d incubation at 30 °C.

Heterologous Localization of HGT Transporters Using Spinning-Disk Confocal Microscopy. Cells were grown for 16 h in SC-ura plus 2% glucose at 30 °C, harvested, washed, and resuspended in PBS. The preferential cell wall stain Wheat Germ Agglutinin, Alexa Fluor 594 conjugate (Life Technologies) was added to a final concentration of 10 μg mL^{-1} and cells were observed by spinning-disk confocal microscopy. Microscopy was performed using an Olympus IX81 inverted microscope and CSU-X1 Spinning Disk unit (Yokogawa); 488-nm and 561-nm solid-state lasers were used in combination with an 100×/1.40 oil objective. A Photometrics CoolSNAP HQ2 camera (Roper Scientific) and the VisiView software package (Visitron Systems) were used for imaging.

Competitive Assays. Competitive assays were performed using *S. cerevisiae* W303 strains engineered to constitutively express GFP (CAY195) or BFP (CAY173) at the endogenous URA3 locus. These fluorescent tags were chosen as the BFP fluorophore is a result of a single amino acid substitution (Y66F), and growth assays have demonstrated that they maintain similar growth dynamics (*SI Appendix*, Fig. S6). URA3 integration was followed by its replacement with the GFP/BFP cassette by modification of previously described plasmids (68). Positive transformants were selected using 5-Fluoroorotic acid (5-FOA) and strains were back-crossed three times to eliminate random mutations as a result of 5-FOA treatment. *S. cerevisiae* CAY strains, transformed with either p426-GPD or p426-GPD HGT-1/p426-GPD *STL1*, were grown overnight on selective SC-ura agar. Strains were then grown overnight in 5 mL SC-ura (30 °C, 180 rpm) until late logarithmic phase, washed once, and resuspended in water to 2.5×10^7 cells/mL Cells were counted using a Beckman Coulter CytoFLEX S flow cytometer and equal cell numbers (1×10^6) of the reference strain and competing strain were added to 10 mL SC-ura containing 0.1–5% glycerol. At 24-h intervals, cells were resuspended in PBSE (10 mM Na_2HPO_4, 2 mM KH_2PO_4, 137 mM NaCl, 2.7 mM KCl, 0.1 mM EDTA, pH 7.4) containing 1 μg mL^{-1} propidium iodide (to allow the exclusion of dead cells) and analyzed by flow cytometry to calculate live cell numbers for each strain. All analyses were based on three biological replicates.

For competitive assays requiring a carbon source switch at 12-h intervals, 1 mL of each 10-mL culture was removed, centrifuged at 17,000 × *g* for 5 min, and suspended in a new 10-mL culture containing the replacement carbon source. An additional 1 mL of each culture was also removed, suspended in PBSE and 1 μg mL^{-1} propidium iodide (to exclude dead cells), and assayed by flow cytometry, as above. Competitive growth assays were analyzed using a generalized linear model with a binomial error distribution. The analysis was performed in R v3.1.2 (R Core Team 2014). Cell counts for each competing strain (expressed as proportions), 72 h after mixed-genotype populations were established, were used for the response variable. The model included a three-way interaction between substrate, concentration, and type of competition (i.e., an HGT-1 expressing strain versus a p426-GPD vector-only control strain or a Stl1p expressing strain).

^{14}C Glycerol Accumulation. *S. cerevisiae* strains were grown for 16 h at 30 °C shaking. Cells were then diluted, grown until early log-phase, and then harvested by centrifugation at 3,000 × *g* for 5 min. The weight of each sample was recorded and cells were washed twice and suspended in water. Ten-microliters of cells were added to 10 μL Tris/citrate buffer (pH 5.0) and cells were allowed to equilibrate to 30 °C. [^{14}C(U)]-glycerol (Perkin-Elmer) was added to a final concentration of 1 mM and cells were incubated at 30 °C for 30 min. At intervals, cells were quenched by the addition of 1 mL ice-cold water and collected by centrifugation at 14,000 × *g* for 3 min. Cells were washed once, suspended in 500 μL of water, and added to 2.5-mL emulsifier-safe scintillation mixture solution (Perkin-Elmer). Radioactivity was determined in a liquid scintillation analyzer (Beckman Coulter LS 6500), and all analyses were based on three biological replicates.

ACKNOWLEDGMENTS. We thank Prof. Eckhard Boles for the gift of the *Saccharomyces cerevisiae* EBY.VW4000 strain; Dr. Cat Gadelha for the p426 GPD sfGFP vector; Prof. Ken Haynes' laboratory for the *S. cerevisiae* BY4742 strain and reagents for transformations/Western blots; Dr. Varun Varma for his advice on statistical analyses; and Emma Chapman for her technical assistance. F.M. is supported by a Genome Canada fellowship; C.A.M. is supported by Biotechnology and Biological Sciences Research Council Grant BB/N016858/1; and T.A.R. is supported by a Royal Society University Research Fellowship (UF130382). This work is supported mainly by funding from a Philip Leverhulme award from the Leverhulme Trust (PLP-2014-147), with additional support from The Gordon and Betty Moore Foundation (Grant GBMF5514). The University of Exeter OmniLog system and associated operations were supported by a Wellcome Trust Institutional Strategic Support Award WT105618MA.

1. Ochman H, Lawrence JG, Groisman EA (2000) Lateral gene transfer and the nature of bacterial innovation. *Nature* 405:299–304.
2. Popa O, Hazkani-Covo E, Landan G, Martin W, Dagan T (2011) Directed networks reveal genomic barriers and DNA repair bypasses to lateral gene transfer among prokaryotes. *Genome Res* 21:599–609.
3. Keeling PJ, Palmer JD (2008) Horizontal gene transfer in eukaryotic evolution. *Nat Rev Genet* 9:605–618.
4. McCarthy CG, Fitzpatrick DA (2016) Systematic search for evidence of interdomain horizontal gene transfer from prokaryotes to oomycete lineages. *MSphere* 1:e00195-16.
5. Richards TA, Dacks JB, Jenkinson JM, Thornton CR, Talbot NJ (2006) Evolution of filamentous plant pathogens: Gene exchange across eukaryotic kingdoms. *Curr Biol* 16: 1857–1864.
6. Richards TA, et al. (2011) Horizontal gene transfer facilitated the evolution of plant parasitic mechanisms in the oomycetes. *Proc Natl Acad Sci USA* 108:15258–15263.
7. Misner I, Blouin N, Leonard G, Richards TA, Lane CE (2014) The secreted proteins of *Achlya hypogyna* and *Thraustotheca clavata* identify the ancestral oomycete secretome and reveal gene acquisitions by horizontal gene transfer. *Genome Biol Evol* 7: 120–135.
8. Belbahri L, Calmin G, Mauch F, Andersson JO (2008) Evolution of the cutinase gene family: Evidence for lateral gene transfer of a candidate *Phytophthora* virulence factor. *Gene* 408:1–8.
9. Wisecaver JH, Rokas A (2015) Fungal metabolic gene clusters-caravans traveling across genomes and environments. *Front Microbiol* 6:161.
10. Marcet-Houben M, Gabaldón T (2010) Acquisition of prokaryotic genes by fungal genomes. *Trends Genet* 26:5–8.
11. Slot JC, Rokas A (2011) Horizontal transfer of a large and highly toxic secondary metabolic gene cluster between fungi. *Curr Biol* 21:134–139.
12. Coelho MA, Gonçalves C, Sampaio JP, Gonçalves P (2013) Extensive intra-kingdom horizontal gene transfer converging on a fungal fructose transporter gene. *PLoS Genet* 9:e1003587.
13. Doolittle WF (1999) Lateral genomics. *Trends Cell Biol* 9:M5–M8.
14. Jain R, Rivera MC, Moore JE, Lake JA (2003) Horizontal gene transfer accelerates genome innovation and evolution. *Mol Biol Evol* 20:1598–1602.
15. Wisecaver JH, Slot JC, Rokas A (2014) The evolution of fungal metabolic pathways. *PLoS Genet* 10:e1004816.
16. Gojković Z, et al. (2004) Horizontal gene transfer promoted evolution of the ability to propagate under anaerobic conditions in yeasts. *Mol Genet Genomics* 271:387–393.
17. Hall C, Brachat S, Dietrich FS (2005) Contribution of horizontal gene transfer to the evolution of *Saccharomyces cerevisiae*. *Eukaryot Cell* 4:1102–1115.
18. Hall C, Dietrich FS (2007) The reacquisition of biotin prototrophy in *Saccharomyces cerevisiae* involved horizontal gene transfer, gene duplication and gene clustering. *Genetics* 177:2293–2307.
19. Marsit S, et al. (2015) Evolutionary advantage conferred by an eukaryote-to-eukaryote gene transfer event in wine yeasts. *Mol Biol Evol* 32:1695–1707.
20. Savory FR, Milner DS, Miles DC, Richards TA (2018) Ancestral function and diversification of a horizontally acquired oomycete carboxylic acid transporter. *Mol Biol Evol* 35:1887–1900.
21. Alexander WG, Wisecaver JH, Rokas A, Hittinger CT (2016) Horizontally acquired genes in early-diverging pathogenic fungi enable the use of host nucleosides and nucleotides. *Proc Natl Acad Sci USA* 113:4116–4121.
22. Gonçalves C, et al. (2018) Evidence for loss and reacquisition of alcoholic fermentation in a fructophilic yeast lineage. *eLife* 7:e33034.
23. Wisecaver JH, Alexander WG, King SB, Hittinger CT, Rokas A (2016) Dynamic evolution of nitric oxide detoxifying flavohemoglobins, a family of single-protein metabolic modules in bacteria and eukaryotes. *Mol Biol Evol* 33:1979–1987.
24. Husnik F, McCutcheon JP (2018) Functional horizontal gene transfer from bacteria to eukaryotes. *Nat Rev Microbiol* 16:67–79.
25. Richards TA, Talbot NJ (2013) Horizontal gene transfer in osmotrophs: Playing with public goods. *Nat Rev Microbiol* 11:720–727.
26. Metcalf JA, Funkhouser-Jones LJ, Brileya K, Reysenbach AL, Bordenstein SR (2014) Antibacterial gene transfer across the tree of life. *eLife* 3:e04266.
27. Moran Y, Fredman D, Szczesny P, Grynberg M, Technau U (2012) Recurrent horizontal transfer of bacterial toxin genes to eukaryotes. *Mol Biol Evol* 29:2223–2230.
28. Lercher MJ, Pál C (2008) Integration of horizontally transferred genes into regulatory interaction networks takes many million years. *Mol Biol Evol* 25:559–567.
29. Cohen O, Gophna U, Pupko T (2011) The complexity hypothesis revisited: Connectivity rather than function constitutes a barrier to horizontal gene transfer. *Mol Biol Evol* 28:1481–1489.
30. Jain R, Rivera MC, Lake JA (1999) Horizontal gene transfer among genomes: The complexity hypothesis. *Proc Natl Acad Sci USA* 96:3801–3806.
31. Savory F, Leonard G, Richards TA (2015) The role of horizontal gene transfer in the evolution of the oomycetes. *PLoS Pathog* 11:e1004805.
32. Cheeseman K, et al. (2014) Multiple recent horizontal transfers of a large genomic region in cheese making fungi. *Nat Commun* 5:2876.
33. Richards TA, Talbot NJ (2018) Osmotrophy. *Curr Biol* 28:R1179–R1180.
34. Goffeau A, et al. (1996) Life with 6000 genes. *Science* 274:546, 563–547.
35. Richards TA, et al. (2009) Phylogenomic analysis demonstrates a pattern of rare and ancient horizontal gene transfer between plants and fungi. *Plant Cell* 21:1897–1911.
36. Soanes D, Richards TA (2014) Horizontal gene transfer in eukaryotic plant pathogens. *Annu Rev Phytopathol* 52:583–614.
37. Spatafora JW, et al. (2016) A phylum-level phylogenetic classification of zygomycete fungi based on genome-scale data. *Mycologia* 108:1028–1046.
38. Risinger AL, Cain NE, Chen EJ, Kaiser CA (2006) Activity-dependent reversible inactivation of the general amino acid permease. *Mol Biol Cell* 17:4411–4419.
39. Cotton JA, McInerney JO (2010) Eukaryotic genes of archaebacterial origin are more important than the more numerous eubacterial genes, irrespective of function. *Proc Natl Acad Sci USA* 107:17252–17255.
40. Stark C, et al. (2006) BioGRID: A general repository for interaction datasets. *Nucleic Acids Res* 34:D535–D539.
41. Huh WK, et al. (2003) Global analysis of protein localization in budding yeast. *Nature* 425:686–691.
42. Yamauchi S, et al. (2015) Opt2 mediates the exposure of phospholipids during cellular adaptation to altered lipid asymmetry. *J Cell Sci* 128:61–69.
43. Homann OR, Cai H, Becker JM, Lindquist SL (2005) Harnessing natural diversity to probe metabolic pathways. *PLoS Genet* 1:e80.
44. Toivari MH, Salusjärvi L, Ruohonen L, Penttilä M (2004) Endogenous xylose pathway in *Saccharomyces cerevisiae*. *Appl Environ Microbiol* 70:3681–3686.
45. Reznicek O, et al. (2015) Improved xylose uptake in *Saccharomyces cerevisiae* due to directed evolution of galactose permease Gal2 for sugar co-consumption. *J Appl Microbiol* 119:99–111.
46. Kasahara M, Shimoda E, Maeda M (1997) Amino acid residues responsible for galactose recognition in yeast Gal2 transporter. *J Biol Chem* 272:16721–16724.
47. Bungay HR (1981) *Energy, the Biomass Options* (Wiley, New York).
48. Heavner BD, Smallbone K, Price ND, Walker LP (2013) Version 6 of the consensus yeast metabolic network refines biochemical coverage and improves model performance. *Database* 2013:bat059.
49. Mattenberger F, Sabater-Muñoz B, Hallsworth JE, Fares MA (2017) Glycerol stress in *Saccharomyces cerevisiae*: Cellular responses and evolved adaptations. *Environ Microbiol* 19:990–1007.
50. Ferreira C, et al. (2005) A member of the sugar transporter family, Stl1p is the glycerol/H+ symporter in *Saccharomyces cerevisiae*. *Mol Biol Cell* 16:2068–2076.
51. McDonald SM, Plant JN, Worden AZ (2010) The mixed lineage nature of nitrogen transport and assimilation in marine eukaryotic phytoplankton: A case study of *micromonas*. *Mol Biol Evol* 27:2268–2283.
52. McDonald TR, Dietrich FS, Lutzoni F (2012) Multiple horizontal gene transfers of ammonium transporters/ammonia permeases from prokaryotes to eukaryotes: Toward a new functional and evolutionary classification. *Mol Biol Evol* 29:51–60.
53. Monier A, et al. (2012) Phosphate transporters in marine phytoplankton and their viruses: Cross-domain commonalities in viral-host gene exchanges. *Environ Microbiol* 14:162–176.
54. Katoh K, Standley DM (2013) MAFFT multiple sequence alignment software version 7: Improvements in performance and usability. *Mol Biol Evol* 30:772–780.
55. Capella-Gutiérrez S, Silla-Martínez JM, Gabaldón T (2009) trimAl: A tool for automated alignment trimming in large-scale phylogenetic analyses. *Bioinformatics* 25: 1972–1973.
56. Price MN, Dehal PS, Arkin AP (2010) FastTree 2—Approximately maximum-likelihood trees for large alignments. *PLoS One* 5:e9490.
57. Nguyen LT, Schmidt HA, von Haeseler A, Minh BQ (2015) IQ-TREE: A fast and effective stochastic algorithm for estimating maximum-likelihood phylogenies. *Mol Biol Evol* 32:268–274.
58. Kass RE, Raftery AE (1995) Bayes factors. *J Am Stat Assoc* 90:773–795.
59. Foster PG (2004) Modeling compositional heterogeneity. *Syst Biol* 53:485–495.
60. Newton MA, Raftery AE (1994) Approximate Bayesian-inference with the weighted likelihood bootstrap. *J R Stat Soc B* 56:3–48.
61. Wieczorke R, et al. (1999) Concurrent knock-out of at least 20 transporter genes is required to block uptake of hexoses in *Saccharomyces cerevisiae*. *FEBS Lett* 464:123–128.
62. Alberti S, Gitler AD, Lindquist S (2007) A suite of Gateway cloning vectors for high-throughput genetic analysis in *Saccharomyces cerevisiae*. *Yeast* 24:913–919.
63. Thompson JR, Register E, Curotto J, Kurtz M, Kelly R (1998) An improved protocol for the preparation of yeast cells for transformation by electroporation. *Yeast* 14:565–571.
64. Sprouffske K, Wagner A (2016) Growthcurver: An R package for obtaining interpretable metrics from microbial growth curves. *BMC Bioinformatics* 17:172.
65. Schütz M, et al. (2016) Directed evolution of G protein-coupled receptors in yeast for higher functional production in eukaryotic expression hosts. *Sci Rep* 6:21508.
66. Vaas LA, et al. (2013) *opm*: An R package for analysing OmniLog(R) phenotype microarray data. *Bioinformatics* 29:1823–1824.
67. Hothorn T, Bretz F, Westfall P (2008) Simultaneous inference in general parametric models. *Biom J* 50:346–363.
68. Hittinger CT, Carroll SB (2007) Gene duplication and the adaptive evolution of a classic genetic switch. *Nature* 449:677–681.